Frontiers of Information Technology & Electronic Engineering
www.jzus.zju.edu.cn; engineering.cae.cn; www.springerlink.com
ISSN 2095-9184 (print); ISSN 2095-9230 (online)
E-mail: jzus@zju.edu.cn

Doppler ambiguity analysis and suppression for LTE-based passive bistatic radars*

Luo ZUO†, Jun WANG†‡, Gang CHEN

National Laboratory of Radar Signal Processing, Xidian University, Xi'an 710071, China

†E-mail: zuoluo_xidian@163.com; wangjun@xidian.edu.cn

Received Apr. 2, 2020; Revision accepted July 19, 2020; Crosschecked Apr. 1, 2021; Published online July 29, 2021

Abstract: In this study, we provide a detailed analysis of the frequency division duplex long term evolution downlink (FDD LTE DL) signal for passive bistatic radars that use the signal as an illuminator of opportunity. In particular, we analyze the cross-ambiguity function and illustrate its undesired deterministic peaks in the Doppler dimension due to the specific structure of the FDD LTE DL signal. A new adaptive mismatched filtering method is proposed for pre-processing the original reference signal to suppress these undesired deterministic peaks in the range-Doppler processing. The effectiveness of our proposed method is demonstrated via simulations following robustness analysis, showing that all undesired peaks are suppressed below −40 dB, with only 1.7 dB reduction in the main peak.

Key words: Passive bistatic radar (PBR); Long term evolution (LTE); Doppler ambiguity; Range-Doppler processing
https://doi.org/10.1631/FITEE.2000143 **CLC number:** TN958.97

1 Introduction

Passive bistatic radar (PBR) uses available non-cooperative transmitters as illuminators of opportunity to perform target detection and localization (Liu et al., 2019). Without the need for deployment and operation of a specialized transmitter, PBR has many advantages over conventional radars. First, PBR is much cheaper than conventional radars. Second, the PBR receiver is easily transported due to its small size. Moreover, due to its bistatic geometry, radar cross-section (RCS) of a target in a PBR is different from its monostatic RCS, which may aid target detection and classification (Cherniakov, 2008). There has been increasing interest in the possibilities of PBR for exploiting external non-radar transmitters of opportunity as their sources of illumination, such as frequency modulation (FM) (Malanowski et al., 2014), analogue television (ATV) (Chen et al., 2018), digital audio broadcast (DAB) (Edrich et al., 2014), digital video broadcast (DVB) (Edrich et al., 2014), global systems for mobile (GSM) (Tabassum et al., 2016), global navigation satellite system (GNSS) (Zaimbashi, 2016), wireless fidelity (Wi-Fi) (Kabakchiev et al., 2014), and long term evolution (LTE) (Karthik and Blum, 2018; Shamaei et al., 2018). Among these illuminators of opportunity, LTE has attracted much attention for its high resolution and wide coverage.

LTE is a wireless communication technology that offers last-mile broadband wireless access with predictable extensive accessibility (Labib et al., 2017). Due to its wide bandwidth, the use of LTE as a radar source can achieve high resolution in target detection (Cao et al., 2017). With wide coverage, the LTE signal has the advantage of network cooperative detection. Therefore, multiple LTE transmitters can be used to form a PBR networking system to expand the detection range of the system. LTE also employs orthogonal frequency division multiplexing (OFDM) as

‡ Corresponding author
* Project supported by the National Key Laboratory Fund (No. 6142411183302)
ORCID: Luo ZUO, https://orcid.org/0000-0002-3434-6312; Gang CHEN, https://orcid.org/0000-0002-1744-9408

its modulation mode, which promises low sidelobes in the ambiguity function. LTE is designed based on the 3GPP standard, which contains a data frame structure and detailed information of the physical downlink control channel (PDCCH) and cell-specific reference (CSR) signal (Salah et al., 2014). The specific structure of LTE gives rise to undesired deterministic peaks in the cross-ambiguity function (CAF) (Evers and Jackson, 2015), which is performed as cross-correlation of reference and surveillance signals (Liang et al., 2016).

These ambiguous peaks may be treated as real targets, which will cause false alarms. What is more, the ambiguous peaks of a strong target may mask the main lobe of a weak target, resulting in a missing alarm (Abdullah et al., 2016a). As these ambiguous peaks are inherent to the transmitted LTE signal and the transmitted signal is uncontrollable by the PBR system designer, the ambiguous peaks need to be managed at the receiver.

Currently, various mismatched methods have been proposed to deal with the ambiguous peak problem. For example, a method of equalizing the specific pilot signal in the DVB-T signal to suppress the undesired peaks was proposed by Palmer et al. (2013). This method requires the support of prior power information of the CSR signal and PDCCH. Unfortunately, the transmitter information changes according to the external environment, which is beyond the control of the PBR designer; thus, the applicability of this method is limited. The method of Bongioanni et al. (2009) can suppress the ambiguities without the transmitter information. In this method, the mismatched reference signal generated by modifying the original reference signal is used to eliminate the influence of the ambiguous peaks in terms of matched results. However, the modified factor is calculated based on the matched filtering results, which means that the method incurs a high computation cost. Thus, it is not conducive to engineering realization. To solve the ambiguity problem, an adaptive mismatched method based on modifying the original reference signal is proposed here.

In this paper, the study of CAF to the FDD LTE DL signals is first extended. Next, the source of the undesired peaks is confirmed and explained thoroughly by formalizing the analysis of CAF. Then, an adaptive mismatched filtering method based on pre-processing the original reference signals is proposed. The performance of the proposed method is evaluated by simulations. Simulation results show that all the undesired peaks are suppressed below −40 dB, with only a 1.7 dB signal-to-noise ratio (SNR) loss in the main peak.

2 LTE signal overview

The LTE physical layer uses the OFDM technology for downlink data transmission and the single-carrier frequency division multiplexing for uplink data transmission (Abdullah et al., 2016b). To meet the requirements of different communication service environments, LTE supports multiple bandwidths from 1.4 to 20 MHz. Two transmission modes are defined for LTE, i.e., FDD and time division duplex (TDD). FDD operates with uplink (UL) and DL on separate frequency bands without overlapping time slots, while TDD has the same frequency band for UL and DL transmissions (Yin et al., 2018). Detailed introduction to the FDD type signal is given in Section 2.1.

2.1 Signal structure

FDD LTE DL data symbols are concatenated in the time domain to form 0.5 ms slots, 1 ms subframes, and 10 ms radio frames. Slots, subframes, and radio frames each have a constant duration, but the total number of symbols varies according to the type of cyclic prefix (CP). A slot consists of seven symbols for a normal CP or six symbols for an extended CP. The CP is a copy of the end portion of a symbol, inserted at the beginning of the symbol to eliminate interference because of multipath delay propagation (3GPP, 2013). In this study, we discuss the extended CP. Fig. 1 illustrates the time domain of the FDD LTE DL signal. The signal has a hierarchical structure in the time domain, with the most basic component being the OFDM symbol with the constant duration T_s. An OFDM symbol comprises a number of sinusoidal subcarriers, which are mutually orthogonal over a useful duration period T_u. These carriers are cyclically extended by a guard band T_g (the length of a normal CP) to produce extended carriers of the full length, $T_s=T_u+T_g$.

In LTE specification, a number of mutually

orthogonal subcarriers are allocated to the user data in advance, and this allocation is termed a resource block (RB). RBs have both time and frequency dimensions, which are presented by mapping to the resource grid (Fig. 2). The resource element (RE) is the smallest unit in an RB and consists of one OFDM symbol of 15 kHz. The combination of these REs makes up an RB, which has 12 subcarriers by one slot in the time-frequency domains.

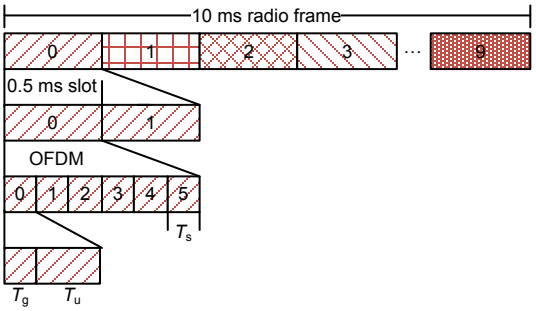

Fig. 1 FDD LTE DL signal frame structure

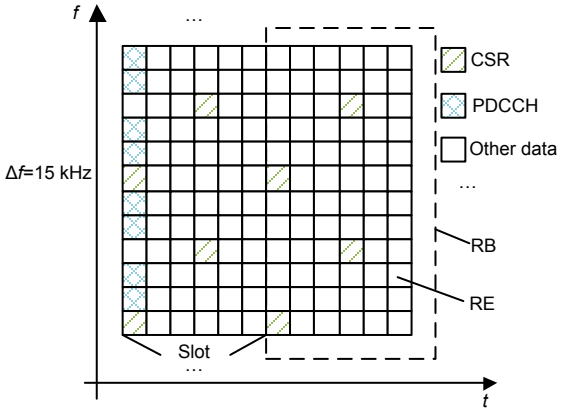

Fig. 2 FDD LTE DL resource grid

The basic frame structure of the FDD LTE DL signal is as described in Fig. 1. Next, the CSR signal and PDCCH will be explained. Their deterministic features affect the range-Doppler (RD) processing results of the LTE signal.

1. CSR signals

The CSR symbols are inserted into the RB to assist the mobile station in channel estimation, demodulation, and decoding of the received signal. The location of the CSR symbol is defined by the LTE standard (3GPP, 2013). Fig. 2 is an illustration of the location of the CRS signal in the FDD LTE DL signal. The CRS signal is distributed in the RB of each subframe, and located at the first and the fourth symbols of one slot. The position of the first occupied subcarrier for the CSR is determined by the physical layer cell identity (CID). CSR signals are placed every six subcarriers (Searle et al., 2014).

2. PDCCH

PDCCH is used for communication between the mobile station and eNodeB. eNodeB initiates a downlink data transmission procedure by sending a scheduling command to the mobile. The scheduling command is written and mapped to PDCCH for transmission using downlink control information (DCI). Fig. 2 shows the location of PDCCH, which occupies the first symbol of each subframe. The starting index of the PDCCH symbols is 1, and these symbols are placed every three subcarriers. When the communication service environment (e.g., the number of cell users and the interference signal of the unit) is stable, the information transmitted by PDCCH is correlated in each subframe. CSR and PDCCH adopt enhanced power modulation quadrature phase shift keying (QPSK). The power is variable according to the actual environment and is not equal to 1.

2.2 Signal definition

The FDD LTE DL signal is formed by the consecutive transmission of individual OFDM symbols. In the OFDM system, the active frequency band is divided into several independent sub-bands. Each sub-band center corresponds to a different subcarrier frequency (Searle et al., 2014). The serial-to-parallel conversion of the modulation code sequence is performed to obtain the parallel modulation sequence corresponding to the subcarrier. Each subcarrier $\psi_k(t)$ is modulated by the parallel modulation sequence (Berger et al., 2010). The baseband structure of the LTE signal with OFDM modulation is given by

$$x(t)=\sum_{j=0}^{J}\sum_{k=0}^{K}R_{jk}\psi_{jk}(t), \tag{1}$$

$$\psi_{jk}(t)=\exp\left[\frac{\mathrm{i}2\pi k(t-T_g-jT_s)}{T_u}\right]q_j(t), \tag{2}$$

where J is the number of symbols per subframe, K is the number of subcarriers depending on the bandwidth, and R_{jk} is the complex-valued modulation symbol. $q(t)$ is a rectangular window of length T_s,

which can be expressed as

$$q(t)=\begin{cases}1, & t\in[-T_{\mathrm{g}},T_{\mathrm{u}}],\\ 0, & \text{otherwise.}\end{cases} \tag{3}$$

Typically, a PBR system works with sampled signals with the sampling frequency $f_{\mathrm{s}}\geq B$, where B is the signal bandwidth and $B=K/T_{\mathrm{u}}$. The discrete LTE signal with OFDM modulation can be written as

$$x[n]=\sum_{j=0}^{J}\sum_{k=0}^{K}R_{jk}\psi_{jk}[n], \tag{4}$$

$$\psi_{jk}[n]=\exp\left[\frac{\mathrm{i}2\pi k(n-N_{\mathrm{g}}-jN_{\mathrm{s}})}{N_{\mathrm{u}}}\right], \tag{5}$$

where N_{g}, N_{u}, and N_{s} are the numbers of samples in the guard bands, useful data, and the total symbol period, respectively.

3 Ambiguity function analysis

The ambiguity function (Venu and Rao, 2017; Dan et al., 2018) is the output of the matched filter between the surveillance signal $\boldsymbol{s}(t)$ and the reference signal $\boldsymbol{r}(t)$:

$$\chi(\tau,f_{\mathrm{d}})=\int_{-\infty}^{+\infty}\boldsymbol{s}(t)\boldsymbol{r}^{*}(t-\tau)\mathrm{e}^{-\mathrm{i}2\pi f_{\mathrm{d}}t}\mathrm{d}t, \tag{6}$$

where τ is the relative temporal delay, f_{d} is the relative Doppler frequency shift, and $(\cdot)^{*}$ denotes the complex conjugate.

In practice, the received signals are sampled, and the matched filtering processing is performed for the windowed signals. The length of the window is called the coherent processing interval (CPI), which determines the Doppler frequency resolution and the coherent integration gain of the PBR system. Direct implementation of the matched filtering processing according to a discrete version of Eq. (6) is computationally expensive. Thus, to lower the computation cost, a typical two-stage pulse-Doppler compression method is adopted to approximate the output as given in Eq. (6). Assuming that the signal is partitioned into M contiguous pulses of length N, the cross-correlations computed at each partition can be represented as

$$\gamma_m[d]=\sum_{n=0}^{N_{\mathrm{cs}}-1}\boldsymbol{s}_m[n]\boldsymbol{r}_m^{*}[n-d], \tag{7}$$

where N_{cs} is the correlation length. From all the pulse compression results, the Doppler dimension can be obtained by taking a discrete Fourier transform (DFT) over the pulses at each delay d:

$$\Xi[d,p]=\sum_{m=0}^{M-1}\gamma_m[d]\exp\left(\frac{-\mathrm{i}2\pi mp}{M}\right), \tag{8}$$

where p is the normalized Doppler unit corresponding to the Doppler frequency.

3.1 Features of the LTE ambiguity function

The ambiguities inherent in the transmitted FDD LTE DL signal are further studied. To highlight the features explained by the analysis, the FDD LTE DL signal at the baseband is simulated to obtain the discrete-time form of CAF. The related parameters are shown in Table 1. Processing is implemented using five radio frames, including 600 symbols. Each symbol contains 2208 or 2192 samples. The matched filtering results are shown in Fig. 3. The strength of the results is normalized with respect to zero delay and a zero Doppler peak. Several ambiguities can be seen aside from the large peak at zero delay and zero Doppler peak. To clearly observe these undesired peaks, Fig. 3b shows the CAF in the Doppler dimension within ±6 kHz, and Fig. 3c shows the CAF after constant false alarm ratio (CFAR) detection. In Fig. 3b, we note that the CAF has one main peak

Table 1 Simulation parameters for the FDD LTE DL signal

Parameter	Symbol	Value
Sampling rate (MHz)	f_{s}	30.7
Transmission type		FDD
Coherent integration time (ms)	T_{c}	50
Bandwidth (MHz)	B	20
Cyclic prefix type		Extended
Cyclic prefix duration (μs)	T_{g}	16.67
Data symbol duration (μs)	T_{u}	66.67
Number of data subcarriers	K	1800
Number of symbols per radio frame		120
CSR/PDCCH SNR (dB)		6
Reference signal SNR (dB)		20

surrounded by numerous ambiguity peaks redundant every 1 kHz, and that the SNRs of the ambiguities at 2, 4, and 6 kHz locations are greater than others.

In a real situation, the LTE station transmits a power of about 30 W, and the antenna gain is about 15 dB. Assuming that the LTE carrier frequency is 2.5 GHz and that the bandwidth is 20 MHz, the effective detection range of the LTE station for targets with RCS of 1–10 m^2 is 15–30 km according to the bistatic radar equation. When the radar monitoring target is an airplane (military drone or civil aviation), the required velocity range of observation is 50–360 m/s. The relationship between the radial velocity and the Doppler shift is expressed as follows (Cherniakov et al., 2006):

$$f_{\mathrm{d}} = (2v/c) f_0, \tag{9}$$

where c denotes the speed of light, f_0 is the carrier frequency, and f_0=2.5 GHz. Thus, the Doppler frequency corresponding to the velocity is 0.83–6.00 kHz, which bridges the unambiguous Doppler frequency of 1 kHz. Meanwhile, note that the minimum SNR of these ambiguities is −22 dB and that the maximum reaches −17 dB, which means that these ambiguities may mask the signal reflected from real targets, causing missing alarms. Furthermore, for targets such as military drones with speeds between 50 and 60 m/s, the corresponding Doppler frequency is 0.83–1.00 kHz. Note that although the target Doppler frequency is lower than the unambiguous Doppler frequency of 1 kHz (it can be detected unambiguously), ambiguities with Doppler frequencies greater than 1 kHz will induce false alarms. Thus, the detection ability of the PBR system will be seriously reduced.

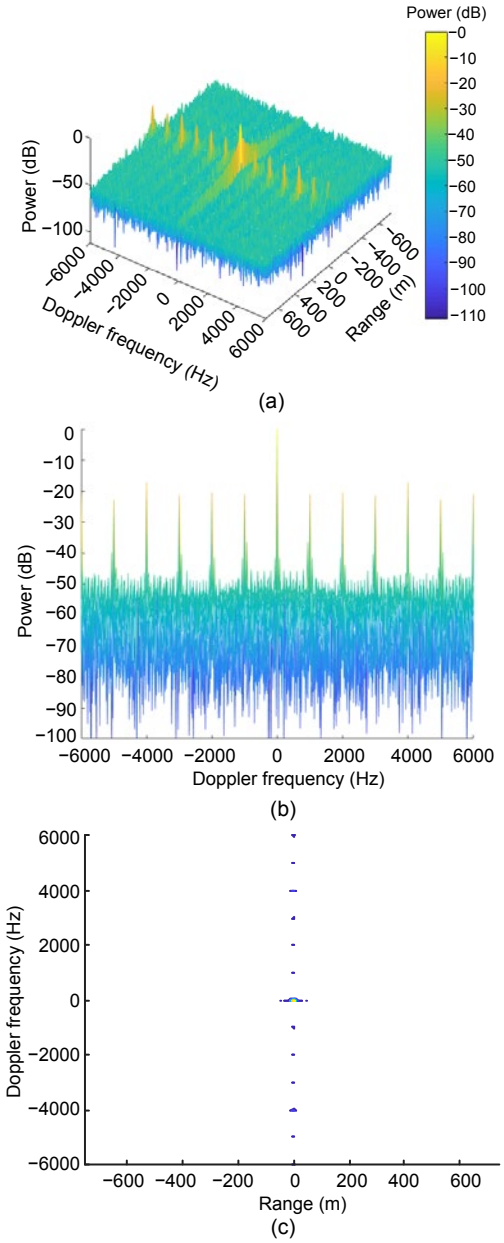

Fig. 3 Matched filtering results of the LTE signal: (a) 3D RD results; (b) 2D RD results in the Doppler dimension; (c) 2D RD results after CFAR detection

The analysis of the LTE signal begins with the two-stage pulse-Doppler compression method. We assume that the CPI is $T_{\mathrm{cpi}}=HT_{\mathrm{c}}$, where T_{c} is the length of the subframe and T_{c}=1 ms, and H is the number of subframes. Moreover, each subframe contains J OFDM symbols of N samples; thus, the signal contains $M=HJ$ OFDM symbols within the CPI. The index of the total number of OFDM symbols is presented as

$$m = j + hJ. \tag{10}$$

As described in Section 2.1, when the physical layer CIDs and the cell communication service environment are fixed, the CSR signal and PDCCH information appear periodically in each slot and subframe, respectively. The cross-correlation results of different pulses in the same delay is written as

$$\gamma_m[d] = \gamma_{m+J}[d]. \tag{11}$$

The CAF of the FDD LTE DL signal can be obtained by applying DFT to the cross-correlation:

$$\Xi[d,p]=\sum_{h}^{H}\exp\left(\frac{-\mathrm{i}2\pi phJ}{M}\right)\sum_{m=0}^{J-1}\gamma_m[d]\exp\left(\frac{-\mathrm{i}2\pi mp}{M}\right)$$
$$=\frac{\sin\frac{\pi pHJ}{M}}{\sin\frac{\pi pJ}{M}}\sum_{m=0}^{J-1}\gamma_m[d]\exp\left(\frac{-\mathrm{i}2\pi mp}{M}\right). \tag{12}$$

According to Eq. (12), the cross-correlation results will cause periodic peaks in the CAF at the Doppler dimension. Substituting Eqs. (4) and (5) into Eq. (12), we have

$$\Xi[d,p]=\frac{\sin\frac{\pi pHJ}{M}}{\sin\frac{\pi pJ}{M}}\sum_{m=0}^{J-1}\gamma_m[d]\exp\left(\frac{-\mathrm{i}2\pi mp}{M}\right)$$
$$=\frac{\sin\frac{\pi pHJ}{M}}{\sin\frac{\pi pJ}{M}}\sum_{m=0}^{J-1}\sum_{n=0}^{N_{\mathrm{cs}}-1}\sum_{k=0}^{K-1}\boldsymbol{S}_{mk}\exp\left[\frac{\mathrm{i}2\pi k(n-N_{\mathrm{g}})}{N_{\mathrm{u}}}\right]$$
$$\cdot\sum_{k'=0}^{K-1}\boldsymbol{S}_{mk'}^{*}\exp\left(\frac{-\mathrm{i}2\pi k'(n-N_{\mathrm{g}}-d)}{N_{\mathrm{u}}}\right)\exp\left(\frac{-\mathrm{i}2\pi mp}{M}\right), \tag{13}$$

where $\boldsymbol{S}_{mk}$ is the modulation codeword sequence.

Due to the orthogonality of the subcarriers within a symbol period, the summation over n reduces to N_{u} when $k=k'$, and 0 otherwise. Thus, Eq. (13) can be further expressed as

$$\Xi[d,p]=$$
$$\frac{\sin\frac{\pi pHJ}{M}}{\sin\frac{\pi pJ}{M}}\sum_{m=0}^{J-1}\sum_{k=0}^{K-1}\left|\boldsymbol{S}_{mk}\right|^2\exp\left(\frac{-\mathrm{i}2\pi kd}{N_{\mathrm{u}}}\right)\exp\left(\frac{-\mathrm{i}2\pi mp}{M}\right). \tag{14}$$

The CAF of the FDD LTE DL signal has a maximum value when $d=p=0$. However, due to the CSR signal and PDCCH, $\Xi[d, p]$ is not a thumbtack standard ambiguity function. In the following analysis, the features of the CAF in the Doppler dimension are discussed.

When $d=0$ and $p\neq 0$, the CAF of the FDD LTE DL signal can be rewritten as

$$\Xi[0,p]=\frac{\sin\frac{\pi pHJ}{M}}{\sin\frac{\pi pJ}{M}}\sum_{m=0}^{J-1}\sum_{k=0}^{K-1}\left|\boldsymbol{S}_{mk}\right|^2\exp\left(\frac{-\mathrm{i}2\pi mp}{M}\right). \tag{15}$$

The ambiguity function (15) is closely related to the ambiguous characteristics of the modulation codeword sequence $\boldsymbol{S}_{mk}$. The acyclic autocorrelation function of $\boldsymbol{S}_{mk}$ determines the amplitude of LTE CAF in the Doppler profile. Furthermore, $\boldsymbol{S}_{mk}$ is composed mainly of user data $\boldsymbol{S}_{m_{\mathrm{user}}k_{\mathrm{user}}}$, CSR signal $\boldsymbol{S}_{m_{\mathrm{csr}}k_{\mathrm{csr}}}$, and PDCCH $\boldsymbol{S}_{m_{\mathrm{pdcch}}k_{\mathrm{pdcch}}}$. Thus, the amplitude of the ambiguity peaks is determined by $\boldsymbol{S}_{m_{\mathrm{csr}}k_{\mathrm{csr}}}$ and $\boldsymbol{S}_{m_{\mathrm{pdcch}}k_{\mathrm{pdcch}}}$. The locations of these peaks are distributed in the integer multiples of the normalized Doppler frequency $p=M/J$. The corresponding Doppler frequency f_{d} of the ambiguous peaks is written as

$$f_{\mathrm{d}}=p/T_{\mathrm{cpi}}=1. \tag{16}$$

The CSR signal and PDCCH lead to ambiguities in the Doppler dimension. The CSR signal and PDCCH are boosted in power, which varies according to the actual communication environment. The amplitude of all symbols $\boldsymbol{S}_{mk}$ is constant with different k's, and particularly for CSR and PDCCH positions j and k specified by the standard, $E[|\boldsymbol{S}_{mk}|^2]\neq 1$. Therefore, terms corresponding to the CSR signal and PDCCH will contribute to $\Xi[0, p]$. We emphasize here that the appearance of these peaks due to the CSR signal and PDCCH satisfies two conditions: codeword power $E[|\boldsymbol{S}_{mk}|^2]\neq 1$ and its specific location. The ambiguities caused by the CSR signal and PDCCH are discussed in detail in the next two subsections.

3.2 Ambiguities caused by the CSR signal

According to Eq. (16), ambiguities may potentially appear at an integer multiple of 1 kHz. As described in Section 2.1, CSR signals are located every six carriers in a symbol and occupy every three symbols in the carrier (Fig. 2). Thus, the ambiguity peaks caused by the CSR signal can be written as

$$\Xi_{\mathrm{csr}}[0,p]=\sin\left(\frac{\pi pH_{\mathrm{csr}}J_{\mathrm{csr}}}{M_{\mathrm{csr}}}\right)\Big/\sin\left(\frac{\pi pJ_{\mathrm{csr}}}{M_{\mathrm{csr}}}\right)$$
$$\cdot\sum_{m_{\mathrm{csr}}=0}^{J_{\mathrm{csr}}-1}\sum_{k_{\mathrm{csr}}=0}^{K_{\mathrm{csr}}-1}\left|\boldsymbol{S}_{m_{\mathrm{csr}}k_{\mathrm{csr}}}\right|^2\exp\left(\frac{-\mathrm{i}2\pi m_{\mathrm{csr}}p}{M_{\mathrm{csr}}}\right), \tag{17}$$

where J_{csr} denotes the number of CSR symbols in each subframe, K_{csr} is the number of CSR signal subcarriers, which depends on the bandwidth, and

M_{csr} and H_{csr} are the numbers of CSR symbols and slots within the CPI, respectively. The Doppler locations of the ambiguity peaks in the CAF are expressed as follows:

$$f_{\mathrm{d:csr}} = y\frac{1}{3T_{\mathrm{s}}} + z\frac{1}{6T_{\mathrm{s}}} + 6q\frac{1}{T_{\mathrm{u}}} = 4y + 2z + 90q \ \text{(kHz)}, \tag{18}$$

where y, z, and q are integers. As shown in Fig. 3, ambiguity peaks at 2, 4, and 6 kHz in the CAF are caused by the CSR. Fig. 3 also clearly shows that the ambiguity peaks at every 2 kHz are greater than other peaks of PDCCH. The ambiguities at every 2 kHz are caused by the CSR signal and PDCCH.

3.3 Ambiguities caused by PDCCH

A similar approach is performed to analyze the ambiguities generated by PDCCH. From Fig. 2, it is observed that PDCCH symbols are uniformly spaced every three carriers and occupy every 12 symbols. Therefore, the ambiguity peaks caused by PDCCH can be presented as

$$\Xi_{\mathrm{pdcch}}[0,p] = \sin\left(\frac{\pi p H_{\mathrm{pdcch}} J_{\mathrm{pdcch}}}{M_{\mathrm{pdcch}}}\right) \Big/ \sin\left(\frac{\pi p J_{\mathrm{pdcch}}}{M_{\mathrm{pdcch}}}\right) \cdot \sum_{m_{\mathrm{pdcch}}=0}^{J_{\mathrm{pdcch}}-1} \sum_{k_{\mathrm{pdcch}}=0}^{K_{\mathrm{pdcch}}-1} \left| \boldsymbol{S}_{m_{\mathrm{pdcch}} k_{\mathrm{pdcch}}} \right|^2 \exp\left(\frac{-\mathrm{i}2\pi m_{\mathrm{pdcch}} p}{M_{\mathrm{pdcch}}}\right), \tag{19}$$

where J_{pdcch} denotes the number of PDCCH symbols in each subframe, K_{pdcch} is the number of PDCCH signal subcarriers, which depends on the bandwidth, and M_{pdcch} and H_{pdcch} are the numbers of PDCCH symbols and subframes within the CPI, respectively. The Doppler locations of the ambiguity peaks in the CAF are expressed as follows:

$$f_{\mathrm{d:dpcch}} = \frac{3y'}{T_{\mathrm{u}}} + \frac{z'}{12T_{\mathrm{s}}} = 45y' + z' \ \text{(kHz)}, \tag{20}$$

where y' and z' are integers. Eq. (20) clearly shows that PDCCH causes ambiguities every 1 kHz. Furthermore, it can be found from Eqs. (17) and (19) that the amplitudes of the ambiguity peaks in CAF $|\Xi[0,p]|$ are produced by the superposition of $|\Xi_{\mathrm{csr}}[0,p]|$ and $|\Xi_{\mathrm{pdcch}}[0,p]|$, respectively, which explains why the amplitudes of the ambiguities at 2, 4, and 6 kHz are greater than others.

In summary, specific features of the CSR signal and PDCCH cause the ambiguities in LTE CAF. The detection performance of the radar system will be severely degraded by these ambiguities when the Doppler shift of a moving target is greater than 1 kHz.

4 Proposed mismatched method

As discussed in Section 3, the reason for ambiguities is that the power and position of CSR and PDCCH satisfy certain conditions. To suppress the ambiguities, the only parameter that can be manipulated is power. In this section, we propose an adaptive mismatched method for pre-processing the original reference signal to suppress the ambiguities caused by a specific CSR signal and PDCCH. Similar to existing methods, a mismatched cross-correlation approach for the LTE DL FDD signal is adopted. The obvious distinction between our proposed method and previous methods (Bongioanni et al., 2009; Palmer et al., 2013) is that our proposed method is adaptable and easy to implement. In Palmer et al. (2013), the modified weight factor was obtained on the premise of known signal modulation information. In Bongioanni et al. (2009), the modified factor was obtained in advance in terms of the matched cross-correlation results. By contrast, the method proposed in this study can calculate the modified factor without prior information of the transmitting signal and the matched cross-correlation results. A simplified block diagram of the proposed method is sketched in Fig. 4.

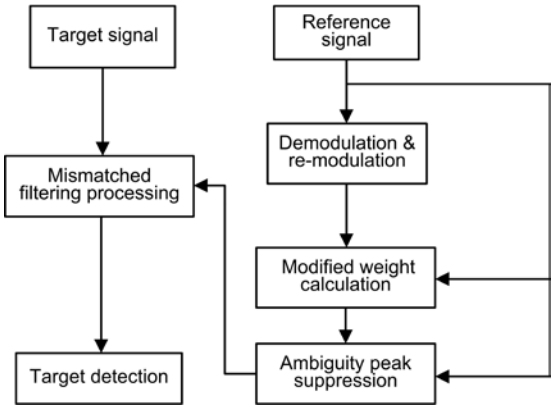

Fig. 4 Proposed pre-processing and mismatched cross-correlation for ambiguity suppression

In this method, the original reference signal is received by a dedicated antenna that directs to the LTE transmitter. First, this reference signal is demodulated to obtain the detailed information of the CSR signal and PDCCH. Then, the specific information of the CSR signal and PDCCH is re-modulated according to the LTE signal standard structure to generate an unambiguous reference signal with 1-power CSR signal and PDCCH, $E[|\boldsymbol{S}_{mk}|^2]=1$.

The unambiguous reference signal can be regarded as a standard template. Next, a Tikhonov regularization optimal model is established between this template signal and the original reference signal to obtain the modified weights of the CSR signal and PDCCH. Finally, the mismatched reference signal is constructed by reducing the amplitude of the CSR signal and PDCCH in the original reference signal to squares of weight.

The modified weights are estimated by solving the Tikhonov regularization optimal problem, which can be regarded as an optimal quadratic problem:

$$\boldsymbol{w}_h = \arg\min_{\boldsymbol{w}_h} \left\| \boldsymbol{r}_h' \boldsymbol{w}_h - \boldsymbol{r}_h \right\|_2^2 + \lambda \left\| \boldsymbol{w}_h \right\|_2^2, \tag{21}$$

where $\boldsymbol{r}_h'$ and $\boldsymbol{r}_h$ are the CSR signal and PDCCH within the h^{th} subframe of the original reference signal and the unambiguous reference signal, respectively, $\boldsymbol{w}_h$ is the modified weight of the CSR signal and PDCCH within the h^{th} subframe of the original reference, $\left\| \boldsymbol{r}_h' \boldsymbol{w}_h - \boldsymbol{r}_h \right\|^2$ denotes the consistency of $\boldsymbol{r}_h$ and $\boldsymbol{r}_h'$, and λ is a constant to control the size of the weight $\|\boldsymbol{w}_h\|^2$, which is used to prevent overfitting. Eq. (21) is a convex quadratic function; therefore, the optimal solution to this problem can be achieved by the zero points of the gradient:

$$\boldsymbol{w}_h = \left[\left(\boldsymbol{r}_h' \right)^{\mathrm{H}} \boldsymbol{r}_h' + \lambda \boldsymbol{I} \right]^{-1} \left(\boldsymbol{r}_h' \right)^{\mathrm{H}} \boldsymbol{r}_h. \tag{22}$$

Thus, the amplitude of the CSR signal and PDCCH in the mismatched reference signal is suppressed by a factor of $\boldsymbol{w}_h^2$ compared with the amplitude of the CSR/PDCCH in the original reference signal. Consequently, contributions to CAF caused by the CSR signal and PDCCH will have 1-power (instead of $\boldsymbol{w}_h^2$), and will no longer be preferential to contributions from user data.

Fig. 5 shows the cross-correlation RD outputs with the mismatched reference signal created by the proposed method and the original matched reference signal (simulation parameters are shown in Table 1). As shown in Fig. 5a, different levels of the ambiguous peaks caused by PDCCH and the CSR signal are all suppressed below −40 dB, which means that the peaks of a real target will not cause false alarms, and that the peaks of a strong target will not mask the main lobe of a weak target. Note that the SNR loss in the main peak is limited (only 0.9 dB), compared with that in the ambiguity peaks.

5 Simulation results

In this section, the target detection performance of the proposed mismatched method was verified by simulations. Two surveillance signals containing different target returns were considered to be received. The related parameters are listed in Table 2.

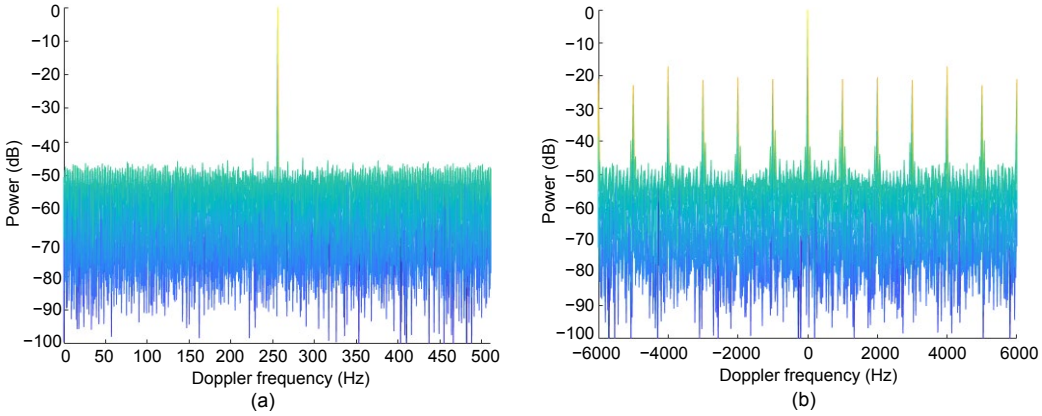

Fig. 5 Cross-correlation range-Doppler frequency outputs of the mismatched reference signal (a) and the original reference signal (b)

5.1 One strong return in the surveillance signal

In this case, target 1 was inserted into the surveillance signal. The results of RD processing, which show both the original reference signal and the mismatched reference signal created by the proposed method, are represented in Fig. 6. Fig. 6a shows that multiple targets appear in the RD processing results due to the ambiguous peaks of the real target. These targets are located at (10 km, 1 kHz), (10 km, 2 kHz), (10 km, 3 kHz), (10 km, 4 kHz), and (10 km, 5 kHz), which results in false targets. In contrast, when the mismatched reference signal is used, the detection of the target is unique, located only at (10 km, 1 kHz).

Table 2 Target return simulation parameters

Signal	SNR (dB)	Range (km)	Doppler frequency (Hz)
Target 1	−20	10	1000
Target 2	−40	10	2000
Target 3	−35	10	4000
Target 4	−30	15	1200
Target 5	−35	15	2200

5.2 Multiple weak returns in the surveillance signal

The strong return of the previous part was retained, and other weak targets, as shown in Table 2, were added. Similar to Fig. 6, Fig. 7 shows the processing results of the original reference and the proposed mismatched reference. Fig. 7 shows that the weak targets are masked by the ambiguous peak of the strong target at the same distance, which causes missing alarms. However, when the mismatched reference is used, the main peak of the targets can be clearly distinguished.

In conclusion, after pre-processing of the original reference signal, all false targets caused by ambiguities are unobservable, and the missing target is detectable. When the radar monitoring object is an airplane (civil aviation or military drone) whose Doppler frequency is greater than the unambiguous Doppler frequency of 1 kHz, the proposed method does well in target detection of LTE-based PBR, which shows the necessity of suppressing the ambiguous peaks.

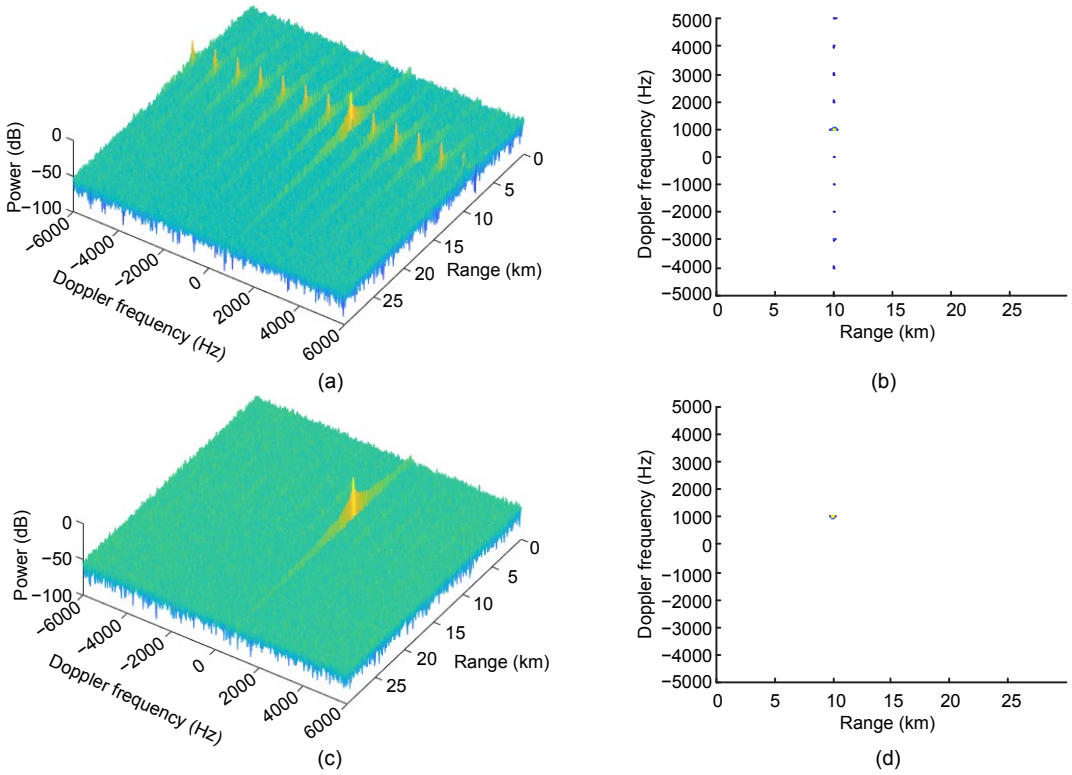

Fig. 6 One strong return target detection results of two methods: (a) 3D RD results of the matched filter; (b) CFAR detection results of the matched filter; (c) 3D RD results of the proposed method; (d) CFAR detection results of the proposed method

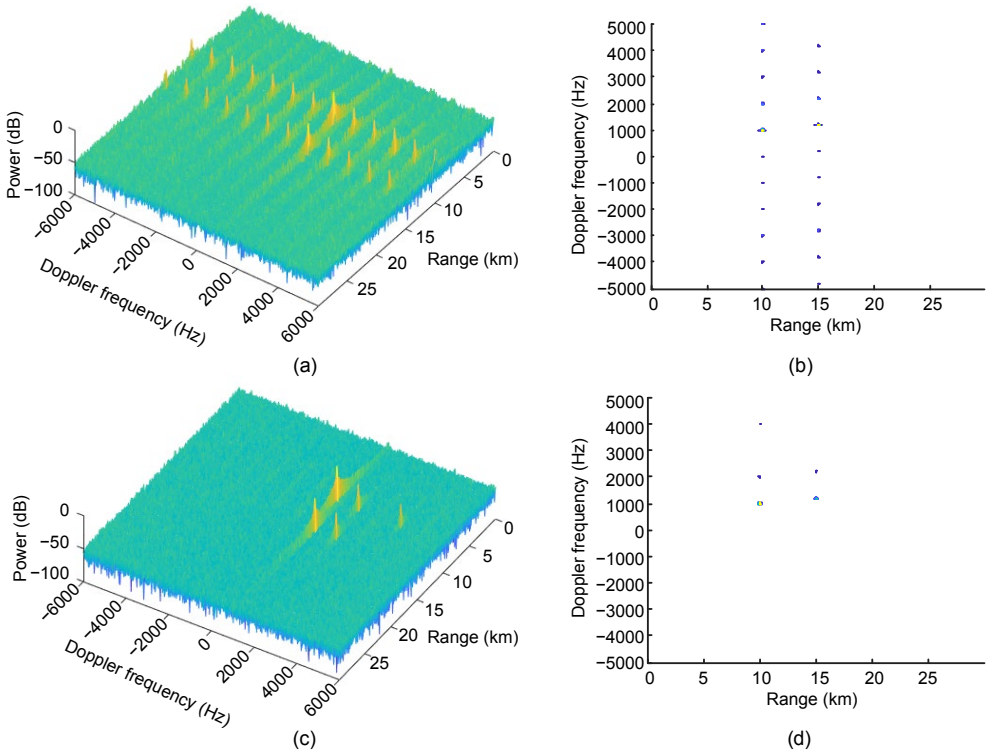

Fig. 7 Multiple weak target detection results of two methods: (a) 3D RD results of the matched filter; (b) CFAR detection results of the matched filter; (c) 3D RD results of the proposed method; (d) CFAR detection results of the proposed method

6 Performance

To further evaluate the performance of the proposed method, additional simulations are conducted. We assume that the unambiguous reference signals are obtained via the demodulation and remodulation operations. Simulation parameters are listed in Table 1.

Note that our proposed method generates a slightly mismatched reference signal with respect to the surveillance signal by pre-processing the original reference signal. The ambiguity peaks are suppressed by applying the mismatched reference signal. The better the suppression performance, the larger the SNR loss (SNRL) in the main peak. SNRL is evaluated as the ratio of the output of the matched filter to the output of the proposed linear mismatched filter. Thus, the numerical value of SNRL can be expressed as

$$\mathrm{SNRL}=\left(\sum_n|\boldsymbol{s}_n|^2\sum_n|\boldsymbol{r}_{\text{mis-}n}|^2\right)\Big/\left|\sum_n\boldsymbol{s}_n\boldsymbol{r}_{\text{mis-}n}\right|^2, \quad (23)$$

where $\boldsymbol{s}_n$ is the surveillance signal and $\boldsymbol{r}_{\text{mis-}n}$ is the mismatched reference signal when calculating SNRL in the main peak. When calculating the loss of ambiguity peaks, $\boldsymbol{s}_n$ represents the CSR signal and PDCCH in the surveillance signal, and $\boldsymbol{r}_{\text{mis-}n}$ denotes the CSR signal and PDCCH in the mismatched reference signal.

According to the simulation parameters shown in Table 1, the average reduction of the ambiguity peaks is about 50 dB and the reduction of the main peak is about 0.9 dB. Simulation results in Fig. 5 are consistent with the calculated numerical values.

Then, the reductions of the ambiguity peaks (average value of the ambiguity peak reduction) and the main peak are analyzed with different CSR/PDCCH power and original reference signal power. The simulation results are presented in Fig. 8. The reduction of the ambiguity peak (Fig. 8a) decreases and then tends to a specific value with increasing reference signal power when the CSR/PDCCH power is fixed. The reduction of the main peak (Fig. 8b) increases and then stabilizes at a specific value with increasing reference signal power when the CSR/

PDCCH power is fixed. Furthermore, note that when the reference signal power is greater than 10 dB, the ambiguity reduction is less than −40 dB, which means that the influence of the ambiguity peaks on target detection can be ignored. The maximum reduction of the main peak is 1.7 dB, which is very small, relative to the reduction in ambiguities.

The suppression capability of the approach can be further illustrated by comparison with the standard matched filter and the existing method (Bongioanni et al., 2009) under 6 dB power of CSR signal and PDCCH. The method of Bongioanni et al. (2009) exploited the knowledge of the pilot carrier position inside the OFDM symbols for the reduction of the undesired deterministic peaks. This method consists of three stages: guard interval blanking, pilot equalization, and pilot blanking. Pilot equalization suppresses the ambiguities caused by the intra-symbol pilots, corresponding to the delay of $\tau<T_u$. The equalization method and the method proposed in this study are performed to obtain the first mismatched reference signal m1 and the second mismatched reference signal m2, respectively. Fig. 9 shows a comparison of these three methods for reducing ambiguities in the CAF of the FDD LTE DL signal. At the 2 kHz peak, a reduction of 4.74 dB from −20.49 to −25.23 dB is obtained when comparing the matched reference with the mismatched reference signal m1. When the mismatched reference signal m2 is applied in the CAF, a reduction of more than 30 dB at the 2 kHz peak to below the pedestal is achieved. Similar results can be seen at other ambiguities.

The simulation results clearly demonstrate the effectiveness of the proposed ambiguity suppression method.

7 Conclusions

In this paper, we presented a detailed analysis of the FDD LTE DL signal in a PBR system. The FDD LTE DL signal with extended CP has a deterministic signal structure that causes undesired peaks in the CAF in the Doppler dimension. These peaks affect the performance of the PBR system as they are treated as real targets, which may cause false or missing alarms in target detection.

The two-stage pulse-Doppler compression method was adopted to approximate the FDD LTE DL signal CAF, and the reason for the undesired peaks

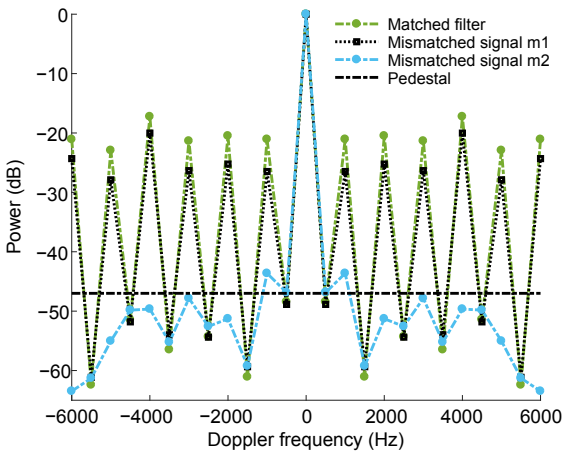

Fig. 9 Comparison of the suppression capability of different methods

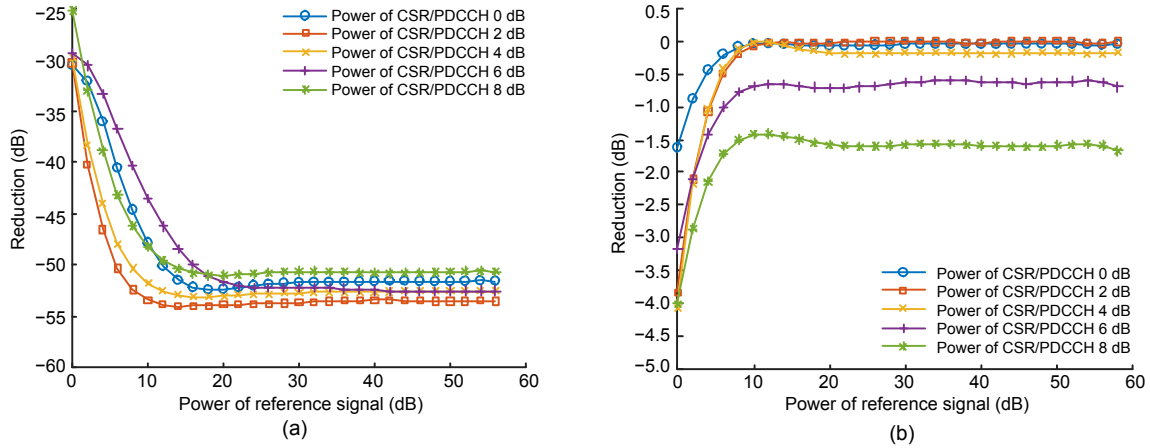

Fig. 8 Reduction versus different reference signal power and CSR/PDCCH power: (a) ambiguity peak reduction; (b) main peak reduction

was explained in detail. Furthermore, a new adaptive mismatched filtering approach was proposed. This approach first obtains an unambiguous reference signal by demodulating and remodulating the original reference signal. The quadratic optimization problem model of these two signals is then established, and the modified weights can be achieved by solving the optimization model. Finally, the unwanted peaks in the LTE CAF are suppressed by modifying the amplitude CSR signal and PDCCH information in the original reference signal. The effectiveness of our proposed method was evaluated using simulations. Results showed that all the undesired peaks are suppressed below −40 dB, and that the SNRL in the main peak is only 1.7 dB.

Contributors

Luo ZUO and Jun WANG designed the research. Luo ZUO processed the data and drafted the manuscript. Jun WANG helped organize the manuscript. Jun WANG and Gang CHEN revised and finalized the paper.

Compliance with ethics guidelines

Luo ZUO, Jun WANG, and Gang CHEN declare that they have no conflict of interest.

References

3GPP, 2013. Evolved Universal Terrestrial Radio Access (E-UTRA); Physical Channels and Modulation. 3GPP TS 36.211.

Abdullah RSAR, Salah AA, Ismail A, et al., 2016a. Experimental investigation on target detection and tracking in passive radar using long-term evolution signal. *IET Radar Sonar Navig*, 10(3):577-585. https://doi.org/10.1049/iet-rsn.2015.0346

Abdullah RSAR, Salah AA, Ismail A, et al., 2016b. Ground moving target detection using LTE-based passive radar. Proc Int Conf on Radar, Antenna, Microwave, Electronics and Telecommunications, p.70-75. https://doi.org/10.1109/ICRAMET.2015.7380777

Berger CR, Demissie B, Heckenbach JÖ, et al., 2010. Signal processing for passive radar using OFDM waveforms. *IEEE J Sel Top Signal Process*, 4(1):226-238. https://doi.org/10.1109/JSTSP.2009.2038977

Bongioanni C, Colone F, Langellotti D, et al., 2009. A new approach for DVB-T cross-ambiguity function evaluation. Proc European Radar Conf, p.37-40

Cao W, Hu WD, Zhang LF, et al., 2017. Pilots-aided LTE reference signal reconstruction in low SNR reference channel for passive sensing. Proc IEEE Asia Pacific Microwave Conf, p.97-100. https://doi.org/10.1109/APMC.2017.8251386

Chen G, Wang J, Guo S, et al., 2018. Improved mismatched filtering for ATV-based passive bistatic radar. *IET Radar Sonar Navig*, 12(6):663-670. https://doi.org/10.1049/iet-rsn.2017.0476

Cherniakov M, 2008. Bistatic Radar: Emerging Technology. John Wiley & Sons, New York, USA, p.620-621. https://doi.org/10.1002/9780470985755

Cherniakov M, Abdullah RSAR, Jancovic P, et al., 2006. Automatic ground target classification using forward scattering radar. *IEE Proc Radar Sonar Navig*, 153(5): 427-437. https://doi.org/10.1049/ip-rsn:20050028

Dan YP, Wan XR, Yi JX, et al., 2018. Ambiguity function analysis of long term evolution transmission for passive radar. Proc 12th Int Symp on Antennas, Propagation and EM Theory, p.1-4. https://doi.org/10.1109/ISAPE.2018.8634255

Edrich M, Schroeder A, Meyer F, 2014. Design and performance evaluation of a mature FM/DAB/DVB-T multi-illuminator passive radar system. *IET Radar Sonar Navig*, 8(2):114-122. https://doi.org/10.1049/iet-rsn.2013.0162

Evers A, Jackson JA, 2015. Cross-ambiguity characterization of communication waveform features for passive radar. *IEEE Trans Aerosp Electron Syst*, 51(4):3440-3455. https://doi.org/10.1109/TAES.2015.140622

Kabakchiev C, Behar V, Garvanov I, et al., 2014. Detection, parametric imaging and classification of very small marine targets emerged in heavy sea clutter utilizing GPS-based forward scattering radar. Proc IEEE Int Conf on Acoustics, Speech and Signal Processing, p.793-797. https://doi.org/10.1109/ICASSP.2014.6853705

Karthik AK, Blum RS, 2018. Improved detection performance for passive radars exploiting known communication signal form. *IEEE Signal Process Lett*, 25(11):1625-1629. https://doi.org/10.1109/LSP.2018.2870341

Labib M, Marojevic V, Reed JH, et al., 2017. Enhancing the robustness of LTE systems: analysis and evolution of the cell selection process. *IEEE Commun Mag*, 55(2):208-215. https://doi.org/10.1109/MCOM.2017.1500706CM

Liang F, Wan XR, Gao F, et al., 2016. Passive detection using orthogonal frequency division multiplex signals of opportunity without multipath clutter cancellation. *IET Radar Sonar Navig*, 10(3):516-524. https://doi.org/10.1049/iet-rsn.2015.0238

Liu SH, Ma YH, Huang YM, 2019. Sea clutter cancellation for passive radar sensor exploiting multi-channel adaptive filters. *IEEE Sens J*, 19(3):982-995. https://doi.org/10.1109/JSEN.2018.2879879

Malanowski M, Kulpa K, Kulpa J, et al., 2014. Analysis of detection range of FM-based passive radar. *IET Radar Sonar Navig*, 8(2):153-159. https://doi.org/10.1049/iet-rsn.2013.0185

Palmer JE, Harms HA, Searle SJ, et al., 2013. DVB-T passive radar signal processing. *IEEE Trans Signal Process*, 61(8):2116-2126. https://doi.org/10.1109/TSP.2012.2236324

Salah AA, Abdullah RSAR, Ismail A, et al., 2014.

Experimental study of LTE signals as illuminators of opportunity for passive bistatic radar applications. *Electron Lett*, 50(7):545-547. https://doi.org/10.1049/el.2014.0237

Searle S, Palmer J, Davis L, et al., 2014. Evaluation of the ambiguity function for passive radar with OFDM transmissions. Proc IEEE Radar Conf, p.1040-1045. https://doi.org/10.1109/RADAR.2014.6875747

Shamaei K, Khalife J, Kassas ZM, 2018. Exploiting LTE signals for navigation: theory to implementation. *IEEE Trans Wirel Commun*, 17(4):2173-2189. https://doi.org/10.1109/TWC.2018.2789882

Tabassum MN, Hadi MA, Alshebeili S, 2016. CS based processing for high resolution GSM passive bistatic radar. Proc IEEE Int Conf on Acoustics, Speech and Signal Processing, p.2229-2233. https://doi.org/10.1109/ICASSP.2016.7472073

Venu D, Rao NVK, 2017. Ambiguity function analysis of broadcast signals for passive radar. Proc 2nd IEEE Int Conf on Recent Trends in Electronics, Information & Communication Technology, p.2026-2029. https://doi.org/10.1109/RTEICT.2017.8256954

Yin L, Li SF, Zhu HB, et al., 2018. Reduced-power almost black subframe based pulse radar spectrum sharing for LTE system. *IEEE Trans Electromag Compat*, 60(5):1223-1230. https://doi.org/10.1109/TEMC.2018.2810250

Zaimbashi A, 2016. Multiband FM-based passive bistatic radar: target range resolution improvement. *IET Radar Sonar Navig*, 10(1):174-185. https://doi.org/10.1049/iet-rsn.2015.0109